



HAL
open science

Deformation structures in the frontal prism near the Japan Trench: Insights from sandbox models

Santanu Bose, Puspendu Saha, James J Mori, Christie Rowe, Kohtaro Ujiie,
Frederick M Chester, Marianne Conin, Christine Regalla, Jun Kameda,
Virginia Toy, et al.

► **To cite this version:**

Santanu Bose, Puspendu Saha, James J Mori, Christie Rowe, Kohtaro Ujiie, et al.. Deformation structures in the frontal prism near the Japan Trench: Insights from sandbox models. *Journal of Geodynamics*, 2015, 89, pp.29 - 38. 10.1016/j.jog.2015.06.002 . hal-02457738

HAL Id: hal-02457738

<https://hal.univ-lorraine.fr/hal-02457738>

Submitted on 28 Jan 2020

HAL is a multi-disciplinary open access archive for the deposit and dissemination of scientific research documents, whether they are published or not. The documents may come from teaching and research institutions in France or abroad, or from public or private research centers.

L'archive ouverte pluridisciplinaire **HAL**, est destinée au dépôt et à la diffusion de documents scientifiques de niveau recherche, publiés ou non, émanant des établissements d'enseignement et de recherche français ou étrangers, des laboratoires publics ou privés.

1
2 Deformation structures in the frontal prism near the Japan Trench: insight
3 from Sandbox Models
4

5 Santanu Bose^{1*}, Puspendu Saha¹, James J. Mori², Christie Rowe³, Kohtaro Ujiie⁴,
6 Frederick M. Chester⁵, Marianne Conin⁶, Christine Regalla⁷, Jun Kameda⁸, Virginia
7 Toy⁹, James Kirkpatrick¹⁰, Francesca Remitti¹¹, J. Casey Moore¹², Monica Wolfson-
8 Schwehr¹³, Yasuyuki Nakamura¹⁴, Anchit Gupta¹⁵
9

10
11 ¹University of Calcutta, Department of Geology, Experimental Tectonic Laboratory,
12 35 Ballygunge Circular Road, Kolkata-700 019 India

13 ²Earthquake Hazards Division, Disaster Prevention Research Institute, Kyoto
14 University Gokasho, Uji Kyoto 611-0011 Japan

15 ³Earth and Planetary Sciences Department, McGill University, 3450 University
16 Street, Montreal, QC H3A 0E8 Canada

17 ⁴Graduate School of Life and Environmental Sciences, University of Tsukuba, 1-1-1
18 Tennodai, Tsukuba 305-0006 Japan

19 ⁵Center for Tectonophysics, Department of Geology and Geophysics, Texas A&M
20 University, College Station TX 77843-3115 USA

21 ⁶EA4098 LaRGE, Université des Antilles et de la Guyane, Pointe-à-Pitre, France.

22 ⁷Department of Geosciences, The Pennsylvania State University, University Park PA
23 16802 USA

24 ⁸ Department of Natural History Sciences, Faculty of Science, Hokkaido University,
25 Sapporo 060-0810, Japan

26 ⁹Department of Geology, University of Otago, 360 Leith Walk, Dunedin 9054 New
27 Zealand

28 ¹⁰Department of Geosciences, Colorado State University, Fort Collins, Colorado,
29 USA

30 ¹¹Dipartimento di Scienzedella Terra, Università di Modena e Reggio Emilia largo, S.
31 Eufemia, 19 41 100 Modena Italy

32 ¹²Department of Earth and Planetary Sciences, University of California Santa Cruz,
33 1156 High, St., Santa Cruz, CA 95064 USA

34 ¹³Center for Coastal and Ocean Mapping, Joint Hydrographic Center, University of
35 New Hampshire, 24 Colovos Road, Durham NH 03824 USA

36 ¹⁴Institute for Research on Earth Evolution, JAMSTEC, Yokohama, Japan

37 ¹⁵Department of Earth Sciences, Indian Institute of Technology, Roorkee- 247667,
38 Uttarakhand India
39
40

41 *Correspondence to: bose.santanu@gmail.com
42

43 **Abstract**

44 We have used sandbox experiments to explore the mechanics of the frontal
45 prism structures documented by new borehole and seismic reflection data from IODP
46 Expedition 343 (JFAST). This study investigated the effects of down-dip (across

47 trench axis) variations in frictional resistance along a decollement on the structural
48 development of frontal wedges near subduction zones. To clarify our understanding
49 on the wedge growth over horst-and-graben structures in the subducting plate near the
50 Japan Trench, we performed sandbox experiments with alternate zone of relatively
51 high and low friction on the basal decollement. Our experiments verify that high
52 frictional resistance on the basal fault is needed to produce the observed internal
53 deformation and fault-and-fold structures in the core samples collected during JFAST.
54 Varying down-dip frictional resistance along the decollement causes a temporal
55 change in the style of internal deformation within the wedge and often gives rise to
56 two distinctive structural domains, separated by a break in the surface slope of the
57 wedge: (i) complexly deformed inner wedge with steep surface slope and (ii) shallow
58 taper outer wedge, characterized by a sequence of imbricate thrusts. Our experiments
59 further demonstrate that the topographic slope-break in the wedge develops when the
60 hinterland part of the wedge essentially stops deforming internally, leading to in-
61 sequence thrusting with the formation of outer wedge with low taper angle. For a
62 series of alternate high and low frictional conditions on the basal fault the slope of the
63 wedge varies temporally between topographic slope-break and uniformly sloping
64 wedge.

65 *Keywords:* sandbox experiments, inner and outer wedge, slope-break, horst-and-
66 graben structure, fault friction

67

68 **1. Introduction**

69 It is now well known that the subduction of bathymetric features in the oceanic
70 plate, e.g., seamounts, aseismic ridges, volcanic plateaus has a strong influence on the
71 development of diverse morphological features and deformation structures in the

72 overriding plate (Domingues et al., 2000; Malavieille, 1984; von Huene and Culotta,
73 1989; von Huene and Lallemand, 1990; Lallemand et al., 1992; Lallemand et al.,
74 1994; von Huene et al., 2004; Park et al., 1999; Wang and Hu, 2006). However, their
75 studies indicate that the styles of deformation in the overriding plate vary with the
76 geometry of bathymetric features in the subducting plate. For example, the subduction
77 of seamounts develops steeper surface slope in the inner wedge than that in the outer
78 wedge (Park et al., 1999; Domingues et al., 2000). On the contrary, the subduction of
79 aseismic ridges develops steep outer wedge slope associated with almost flat inner
80 wedge (Lallemand et al., 1992). Despite dominance of horst-and-graben structure at
81 most trenches, its influence on frontal wedge growth has still remained relatively
82 unexplored. We therefore focus the present work to analyze the impacts of subducted
83 horst-and-graben structures on the evolution of frontal wedge near the Japan Trench.

84 Geophysical investigations along several sections across the Japan Trench
85 (Fig. 1b and c) recorded a series of horst-and-graben structures on the subducting
86 plate beneath the frontal wedge (Tsuru et al., 2002; Kodaira et al., 2012; Nakamura et
87 al., 2013). Moreover, earlier studies have shown that the sediment thickness in the
88 incoming Pacific plate near the Japan Trench is thin and the thinning of sediment
89 cover mostly occurs above the horst block (Groshong, 2006). The combination of the
90 effects of the differences in sediment thickness and surface roughness over horst-and-
91 graben structure in the subducting plate cause varying degrees of coupling at the plate
92 interface, creating varying frictional properties on the decollement (Pacheco et al.,
93 1993; Tanioka et al., 1997; von Huene et al., 1999; Bilek, 2007; Das and Watts,
94 2009). In the present study we have used sandbox experiments to simulate the effects
95 of down-dip variations in the frictional strength on the basal decollement to
96 investigate the structural development of frontal wedge and finally, provide a

97 mechanical model for explaining the structural evolution of frontal wedge over horst
98 and graben structure near the Japan Trench.

99 Integrated Ocean Drilling Program (IODP) Expedition 343 (JFAST) drilled to a
100 depth of 836 meters below seafloor (mbsf) near the Japan Trench at site C0019
101 through the plate boundary fault zone over the horst block, located about ~ 6 km
102 westward from the trench axis (Fig. 1a). Core samples collected during the expedition
103 have provided a great opportunity to compare our experimental results with the
104 observed deformation structures within the frontal wedge (Chester et al., 2013,
105 Kirkpatrick et al., 2014). Borehole data and associated seismic images provide new
106 structural information that has been modeled in this study to show the effects of
107 friction on the megathrust near the Japan Trench.

108 .

109 **2. Experimental methods and materials**

110 Sandbox experiments have proved to be useful in understanding the mechanics
111 of thin-skinned accretionary wedges using the concept of critical taper theory
112 (Chapple, 1978; Boyer and Elliot, 1982; Davis et al., 1983; Dahlen, 1990). The angle
113 of critical taper is defined by the summation of basal inclination (β) and surface slope
114 (α). According to critical taper model, a wedge deforms internally and thereby,
115 increases its taper and at a critically tapered angle the wedge develops internal
116 stresses, leading the wedge on the verge of failure. At this stage, shear stress at the
117 base reaches a value that assists frictional sliding at the decollement (Davis, 1983;
118 Boyer and Elliot, 1982). Theoretically and experimentally it has been shown that the
119 angle of critical taper is proportional to the frictional condition on the basal
120 decollement according to the following equation (Dahlen, 1990):

121
$$\alpha + \beta = (\beta + \mu_b) \left(\frac{1 - \sin \phi_c}{1 + \sin \phi_c} \right) \quad (1)$$

122

123 where, μ_b is the coefficient of static friction on the decollement and ϕ_c is the angle of
124 internal friction of the frontal prism material.

125 In the present study, we have prepared our experimental models over varying
126 down-dip frictional conditions on the decollement to simulate the effect of horst-and-
127 graben structure along the basal decollement (Fig.2). We have considered relatively
128 higher frictional coefficient on the decollement above the horst block because of its
129 enhanced surface irregularities due to little or no sediment cover, leading to a strong
130 coupling with the overriding plate than that over the graben sediments. Thus the horst
131 and graben structure gives rise to alternate zones of relatively strong and a weak
132 contact respectively with the overriding plate on the decollement. In the laboratory
133 scaled experiments the higher basal friction ($\mu_b = 0.46$), simulating the decollement
134 immediately above the horst block, was achieved by pasting commercial sand paper
135 (P30, average grit size 622.0 microns) on a glass plate and a relatively lower basal
136 friction ($\mu_b = 0.36$) was obtained by sieving a veneer of boric acid powder (0.001mm
137 beads) over the glass plate in order to model the frictional strength above the graben
138 sediments. However, in some experiments we pasted rigid block of 5mm thick acrylic
139 sheet over the basal glass plate to model the horst block. However, in the second set
140 of experiments, we had to stop the experiment once the buttress reached the edge of
141 the acrylic block. Experimental results from these two different sets of experiments,
142 however, show that frontal wedge propagation ceases once the decollement
143 propagation reaches the high frictional patch / edge of the rigid acrylic sheet (see
144 electronic supplementary Fig. S1). This finding suggests that the use of high frictional

145 patch on the basal glass plate is a suitable analog for simulating natural horst-block.
146 The advantage of using sandpaper over rigid block is that the hinterland buttress can
147 override the high frictional patch without limiting the amount of shortening during the
148 experimental run.

149 In the model setup, Zone I represents a graben in the seismogenic plate interface
150 and Zone II corresponds to a horst block in the subducting plate (Fig. 2). Although a
151 majority of our experiments were carried out with one high frictional patch between
152 zones of relatively lower friction on the basal fault, a few experiments were carried
153 out with two zones of high frictional patches to understand the effects of a series of
154 horst-and-graben structures. Experimental models were prepared by sieving sand
155 layers from a constant height of 20 cm in a rectangular glass-walled sandbox
156 apparatus over a rigid base of varying basal friction (μ_b) (Fig. 2). The length and
157 width of the apparatus are 110 cm and 35 cm respectively. The model width was more
158 than fifteen times its thickness to avoid the effects of friction at the interface of sand
159 layers and the glass sidewalls (Souloumiac et al., 2012). The coefficients of basal
160 friction (μ_b) were calculated separately from sliding experiments using dry non-
161 cohesive sand. Note that the values of μ_b used in our experiments are merely imposed
162 qualitatively for simulating natural situation that do not claim the exact values for
163 natural analogue. The glass walls of the sandbox were cleaned and dried carefully to
164 remove surface moisture. This process is important in order to prevent sticking of
165 sand to the glass walls. Experiments were carried out in controlled laboratory
166 conditions to avoid the influence of atmospheric moisture contents.

167 We used dry, non-cohesive natural quartz-rich (>90%) sand, texturally matured
168 with well rounded grains (average sphericity of 0.8), as analogue material for scaled
169 model experiments simulating crustal scale brittle deformation (Davis et al., 1983;

170 Mulugeta, 1988; Koyi, 1995; Mandal et al., 1997; Schellart, 2000). The sand material
171 had a bulk density of 1600 kg/m^3 , and a coefficient of internal friction close to 0.57.
172 Our model scales to nature with a ratio of 2.7×10^{-5} , where 1 cm in the model is
173 equivalent to 360 m in nature (Table 1). The cohesion of model material (dry quartz
174 sand) in our experiment is around 20 Pa, which scales to 2 MPa (Gutscher et al.,
175 1998) for unconsolidated marine sediments (Hoshino et al., 1972). The models were
176 deformed in a pure shear box at a uniform velocity of 5 mm / minute using a
177 computer controlled step-up motor by setting a backstop at the rear of the sand layers.
178 Previous studies revealed that buttress geometry is important in the development of
179 wedge geometry in sand layers (Byrne et al., 1988; Persson and Sokoutis, 2002).
180 However, we used planar vertical buttress in our experimental setup in order to model
181 a mono-vergent accretionary wedge observed in the Japan Trench (Mulugeta, 1988;
182 Storti and McClay, 1995; Gutscher et al., 1998; Bose et al., 2009). Although sand
183 layer of 1cm thickness should have been used in our experiments according to the
184 scaling law, we have exaggerated the thickness of sand layers to 2 cm in all
185 experiments for obtaining better resolution of deformation structures as well as to
186 understand the deformation mechanism clearly during the experimental run. However,
187 we ran experiments with sand layers of 1 cm thickness to verify the influence of
188 model thickness in experimental results. These experiments show broad resemblance
189 in the first order geometry of the wedge (see electronic supplementary Fig. S2) and
190 therefore validates the use of 2 cm thick sandlayers in the model experiments. During
191 the experimental run, we photographed through the lateral glass wall continuously
192 after an interval of 5 seconds, keeping the camera at a fixed distance from the model.
193 Model deformations were analyzed from successive photographs taken during the
194 experimental run.

195

196 **3. Experimental Results**

197 Our experiments suggest that the frontal wedge near the Japan Trench has
198 evolved over varying down-dip frictional condition on the decollement during
199 subduction of horst-and-graben. In our experiments, the wedge started to grow above
200 Zone I by in-sequence thrusting at the *initial stage* and developed a gentle surface
201 slope (α) at uniform shortening rate (Figs. 3b-3c, 4a). The vertical growth of the
202 wedge at the backstop attained an almost stationary value when the model was
203 shortened by 5 cm in all experiments (Fig. 4b). At this stage, the frontal propagation
204 of the wedge dominated over the vertical growth through sequential thrusting until the
205 deformation front reached Zone II. During this stage the wedge developed a critical
206 taper, α equals 7.5° (Figs. 3d, 4a), which is closer to the theoretical value of surface
207 slope (α) of 6° obtained from “equation 1” for $\beta = 0$, $\mu_b = 0.36$ and $\phi_c = 0.57$.
208 However, the overestimation of α in the experimental result is self-consistent.

209 The mode of internal deformation and its geometry changed completely when
210 the decollement propagation reached the edge of high frictional patch (Zone II, $\mu_b =$
211 0.42), simulating a horst (Fig. 3e, see electronic supplementary Figs. S1 A [d] and B
212 [d]). At this stage, decollement propagation ceased and the wedge formed over Zone I
213 started deforming internally by increasing the wedge height consistently, developing a
214 steep topographic slope (Fig. 4). This stage of wedge growth has been defined as
215 *intermediate stage* (Figs. 3e-3f). The topographic slope of the wedge at this stage
216 became much higher than the predicted value from “equation 1”, leading the wedge to
217 grow to a super critical state. It is likely that the cessation of decollement propagation
218 promotes the development of supercritical wedge in order to accommodate the
219 amount of horizontal shortening, and eventually facilitates slope failure (Fig. 3f).

220 During this stage experimental models demonstrated mechanical rotation and
221 reorientation of already deformed sand layers in the hanging wall, giving rise to a
222 complex deformation structures within the deforming wedge.

223 With further horizontal shortening, the deformation front crossed the Zone II
224 and propagated onto the region above zone I over low μ_b , simulating another graben,
225 by the process of in-sequence thrusting and eventually, developed a separate wedge
226 with a low angle of taper as expected to occur over low basal friction. Such spatial
227 and temporal variations in the style and intensity of deformation across the wedge
228 finally gave rise to distinct topographic slope-break in the wedge geometry separating
229 the steep inner wedge from the low tapered outer wedge (Figs. 3g-3h and 4a). During
230 the growth of outer wedge, the internal deformation in the inner wedge completely
231 stopped (Fig. 4b) and the horizontal shortening was entirely accommodated by in-
232 sequence thrusting over weak frictional base. For simplicity in description, we describe
233 this stage of wedge growth as *final stage*, which characterizes the development of
234 topographic slope-break with the cessation of internal deformation within the inner
235 wedge. Experiments with varying width of Zone II showed that increasing the width
236 of the Zone II (e.g. 30 cm) required large amount of shortening for the development
237 of the topographic slope-break (Figs. 5 and 4, see electronic supplementary Fig. S3).
238 The development of slope-break in the wedge geometry thus can be treated as a
239 potential indicator for interpreting long term frictional condition on the decollement.

240 Experiments with more than one high frictional patch (Zone II) on the basal
241 fault showed that the surface slope of outer wedge (e.g., the wedge over low μ_b) was
242 increasing progressively with ongoing shortening once the decollement propagation
243 was again resisted by another high frictional patch in the front. As a consequence, the
244 wedge geometry was completely modified along with the destruction of topographic

245 slope-break (Fig. 6h). With further shortening the outer wedge progressively merged
246 with the inner wedge, giving rise to a single wedge with steep uniform surface slope
247 (Fig. 6i). During this process of wedge modification, the inactive inner wedge again
248 resumed to deform by mechanically rotating all preexisting structures and thereby,
249 increasing the complexity of deformation structures towards the hinterland part of the
250 wedge (Fig. 6i, 6k). With continuous shortening, the deformation within this steep
251 wedge completely stopped once the deformation front propagated over another low
252 frictional base in the front with the onset of the development of new outer wedge by
253 in-sequence thrusting (Figs. 6j, 6k). Based on above results, it is evident that the
254 geometry of the frontal wedge is essentially transient with varying down-dip frictional
255 strength on the decollement in tectonically active convergent belts over long time
256 scale.

257

258 **4. Discussion**

259 *4.1 Implication of varying down-dip basal friction*

260 On the basis of the above observations and interpretations on the experimental
261 results we discuss below the role of basal friction in the structural development of
262 frontal wedge near the Japan Trench. Our study reveals that varying down-dip
263 frictional strength on the decollement causes a drastic change in the wedge taper,
264 giving rise to a steep *inner wedge* and gentle *outer wedge*. This lateral change in the
265 surface slope across the wedge separates the entire wedge into two distinctive
266 structural domains: (i) complex internal deformation within *the inner wedge* and (ii)
267 the *outer wedge* is deformed mostly by sequential thrusting. Experimental results
268 show that the growth of the inner wedge begins by in-sequence thrusting over low
269 frictional base following the model of critical angle of taper (Davis et al., 1983;

270 Mulugeta, 1988; Koyi, 1995; Gutscher et al., 1998; Yamada et al., 2006; Bose et al.,
271 2009). However, with ongoing shortening the taper angle of the wedge progressively
272 steepens with the termination of decollement propagation by the increased frictional
273 resistance along the decollement. The steepening of the wedge slope couple with
274 intense internal deformation within it continues until the deformation front crosses
275 from the zone of high to low friction on the basal decollement. The progress of the
276 deformation front over the lower frictional base immediately stops internal
277 deformation within the deformed wedge (Figs. 3g- 3h) and thereby, initiates a
278 renewed phase of in-sequence thrusting in response to continuing horizontal
279 shortening, leading to the development of shallow taper outer wedge. This process of
280 wedge propagation over varying basal friction gives rise to the development of
281 topographic slope-break between the inner and the outer wedges. The characteristic
282 geometry of the slope-break in the tectonic wedge becomes prominent when the
283 wedge front continues to deform over a uniform low frictional base for large
284 horizontal shortening (Fig. 5a-g).

285 *4.2 Interpretation of wedge development near the Japan Trench*

286 The present study has an important implication in understanding the
287 development of frontal wedge near the Japan Trench. Seismic sections across the
288 Japan Trench show that the slope of the frontal prism over horst-and-graben structure
289 changes from 10° in the landward part to 4° towards the trench (Fig. 1b). Comparing
290 our experimental results with seismic data from frontal wedge near the Japan Trench
291 suggest that the varying down-dip frictional strength along the basal decollement
292 caused the present geometry of the wedge and deformation structures within it near
293 the Japan Trench (Fig. 1b and 1c). Our experimental results suggest that the
294 subduction of horst-and-graben structure near the Japan Trench are potential factors

295 for creating varying degree of coupling with the overriding plate that eventually
296 developed the characteristic topographic slope-break. It further reveals that the inner
297 wedge with steep slope over the horst block must have formed prior to the
298 propagation of deformation front over the graben sediments. Our experimental study
299 shows that initiation of growth of the outer wedge over low basal friction deactivates
300 the internal deformation of the inner wedge. This has led to infer that the present day
301 plate convergence near the Japan Trench is accommodating entirely by in-sequence
302 thrusting over the low friction graben sediments. Previous experimental findings
303 (Huiqi et al., 1992; Bose et al., 2009) along with the present study indicate that the
304 occurrence of a series of imbricate thrusts over graben sediments, preserved in the
305 outer wedge of the Japan Trench (Kodaira et al., 2012; Nakamura et al., 2013), have
306 formed over relatively weak decollement (Figs. 7c).

307 The structural interpretations from the drill core samples collected during
308 JFAST and seismic data reveal that the frontal prism lying over the subducted horst
309 block (~ high frictional patch) is structurally chaotic, which is also consistent with the
310 observed deformation structures in our experimental models. The dip of beds
311 measured in the core samples varies from 20° to 80° and they are also traversed by
312 numerous closely spaced core scale faults (Chester et al., 2013; Nakamura et al.,
313 2013; Kirkpatrick, 2014) (Fig. 7). Our experimental results show that the complexity
314 in the internal deformation within the inner wedge increases with the onset of
315 steepening of inner wedge slope when the frontal propagation of the decollement is
316 resisted by the high frictional patch during ongoing shortening (Figs. 3 and 4). This
317 has led to infer that the variably steeply dipping beds in the core samples might have
318 evolved through the process of mechanical rotation of earlier structures within the
319 hanging wall when the decollement propagation was either temporarily stopped or

320 was very slow due to high-frictional resistance along the horst block. Based on above
321 discussions, it appears that subduction of horst-and-graben structure played a crucial
322 role in increasing the complexity of deformation structures observed at the drill site
323 near the Japan Trench. With continued plate convergence over time the deformation
324 front eventually crossed the high frictional patch resulting the break in the surface
325 slope observed between the inner and outer wedges in the frontal prism. In the
326 laboratory experiments, the break in the surface slope of the wedge becomes
327 prominent once the backstop overrides the high frictional patch and consequently,
328 develops outer wedge by in-sequence thrusting (Figs. 3g, 6f and 6j). Comparing our
329 experimental results with seismic images reveal that the buttress (~ backstop in the
330 experimental setup) in the natural situation near the Japan Trench currently lies on the
331 west of the JFAST drilling site towards landward part of the wedge, as also predicted
332 by earlier workers (Tsuru et al., 2002) (Fig. 7b and 7c). Our experimental results
333 further reveal that the observed slope sediments between the inner and outer wedge in
334 the Japan Trench might have accumulated during the growth of supercritical wedge as
335 identified in the *intermediate stage* in experiments and the sediment accumulation
336 continued until the deformation front crossed the horst block (Fig. 3f). This, however,
337 does not rule out the possibility of rotational slumping of the slope sediments at the
338 frontal wedge by later reactivation during the 2011 megaearthquake event (Strasser et
339 al., 2013).

340 The present experimental study has also predicted why there is lack of natural
341 examples of the occurrence of multiple slope-breaks in accretionary prisms.
342 Experiments with two high frictional patches show that the cessation of the
343 propagation of outer wedge by another zone of high frictional patch in the front
344 modifies the wedge geometry thoroughly by mechanical rotation of all pre-existing

345 deformation structures including the zone of topographic slope-break, forming a
346 wedge with a uniformly steep surface slope (Fig. 6). These observations have led to
347 infer that the subduction of the horst block in the Pacific plate lying currently on the
348 east of the Japan Trench will eventually modify the present wedge geometry having a
349 topographic slope –break to a uniformly steep slope.

350

351 **5. Conclusion:**

352 Our main conclusions are as follows:

353

- 354 1) Down-dip frictional variations on the decollement cause temporal and spatial
355 variations in the geometry of the frontal wedge.
- 356 2) Surface slope-break develops when the deformation front crosses from high to
357 low basal friction. The break in the surface slope separates the entire wedge
358 into two distinct structural domains: inner and outer wedges.
- 359 3) The inner wedge is characterized by steep wedge slope and complex internal
360 structures, whereas the outer wedge is deformed by in-sequence thrusting,
361 leading to shallow taper angle.
- 362 4) The experimental models thoroughly explain the structural evolution of the
363 frontal wedge near the Japan Trench observed in seismic images and borehole
364 data.
- 365 5) We interpret that the complexity of internal deformation observed in core
366 samples and localization of steep surface slope towards the landward part of
367 the wedge near the Japan Trench is caused by the cessation of decollement
368 propagation by the horst block in the subducting plate lying beneath JFAST
369 drill site.

370 6) The development of shallow taper outer wedge over the graben sediments by
371 in-sequence thrusting marks the cessation of internal deformation in the rear
372 part of the wedge (~ inner wedge), creating the topographic slope-break near
373 the Japan Trench.

374
375 **Acknowledgement:** We thank scientific and drilling staff on Drilling Vessel *Chikyu*
376 for their constant assistance during the IODP expedition 343. We thank Ylona van
377 Dinther and Marc-Andre Gutscher for their insightful reviews and constructive
378 suggestions for improvement of this work. We also thank W.P. Schellart for his
379 guideline to revise the manuscript. The work is supported by MOES, Govt. of India
380 and DST, Govt. of India grants to SB and PS acknowledge CSIR, India for financial
381 support.

382
383 **References**

- 384
385
386 Bilek,S., 2007. Influence of Subducting Topography on Earthquake Rupture
387 In:T. Dixon and C.Moore(eds.), The Seismogenic Zone of Subduction
388 Thrust Faults, ColumbiaUniversityPress.123.
- 389 Bose, S., Mandal,N., Mukhopadhyay,D.K., Mishra,P. 2009. An unstable
390 kinematic state of theHimalayan tectonic wedge: Evidence from
391 experimental thrust-spacing patterns. J. Struct. Geol., 31,83-91.
- 392 Boyer, S.E., Elliot, D., 1982.Thrustsystems. Am. Assoc. Pet. Geol.. 67,1196-
393 1230.
- 394 Byrne, D.E., Davis D.M., Lynn, R.S., 1998.Loci and maximum size of thrust
395 earthquakes and the mechanics of the shallow region of subduction zones.
396 Tectonics, 7, 833.
- 397 Chapple, W.M., 1978.Mechanics of thin-skinned fold-and-thrust belts. Geol. Soc.
398 Am. Bull.89,1189.
- 399 Chester, F.M., Rowe, C., Ujiie, K., Kirkpatrick, J., Regalla, C., Remitti,

400 F., Moore, J.C., Toy, V., Wolfson-Schwehr, M., Bose, S., Kameda, J., Mori,
401 J.J., Brodsky, E.E., Eguchi, N., Toczko, S., Expedition 343 and 343T
402 Scientists. Structure and composition of the plate-boundary slip zone for the
403 2011 Tohoku-Oki earthquake. *Science* 342, 1208-1211.

404 Dahlen, F.A., 1990. Critical Taper Model of Fold-and-Thrust Belts and
405 Accretionary Wedges. *Annu. Rev. Earth Planet. Sci.* 18, 55-99.

406 Das, S., Watts, A.B., 2009. Effects of subducting seafloor topography on the
407 rupture characteristics of great subduction zone earthquakes. In: S.
408 Lallemand and F. Funiciello (eds.), *Subduction Zone Geodynamics*,
409 Springer-Verlag Berlin Heidelberg 103-118.

410 Davis, D.M., Suppe, J., Dahlen, F.A., 1983. Mechanics of fold-and-thrust belts
411 and accretionary wedges. *J. Geophys. Res.* 88, 1153-1172.

412 Dominguez, S., Malavieille, J., Lallemand, S.E., 2000. Deformation of
413 accretionary wedges in response to seamount subduction: Insights from
414 sandbox experiments. *Tectonics*. 19, 182-196.

415 Groshong, R.H., 2006. 3-D Structural geology: a practical guide to quantitative
416 surface and surface map interpretation. Springer, New York, p 400.

417 Gutscher, M. A., Kukowski, N., Malavieille, J., Lallemand, S., 1998. Material
418 transfer in accretionary wedges from analysis of a systematic series of
419 analog experiments. *J. Struct. Geol.* 20(4), 407-416.

420 Hoshino, K., Koide, H., Inami, K., Iwamura, S., Mitsui, S., 1972. Mechanical
421 properties of Japanese tertiary sedimentary rocks under high confining
422 pressures., *Geol. Surv. of Jpn*, Kawasaki, Japan, p 200.

423 Huiqi, L., McClay, K. R., Powell, D. 1992. Physical models of thrust wedges. In
424 *Thrust tectonics*. Springer Netherlands, 71-81.

425 Kirkpatrick, J. D., Rowe, C. D., Ujiie, K., Moore, J. C., Regalla, C., Remitti, F.,
426 Toy, V., Wolfson-Schwehr, M., Kameda, J., Bose, S., Chester, F. M., 2014.
427 Structure and lithology of the Japan Trench subduction plate boundary
428 fault. *Tectonics*. DOI: 10.1002/2014TC003695.

429 Kodaira, S., No, T., Nakamura, Y., Fujiwara, T., Kaiho, Y., Miura, S., Takahashi,
430 N., Kaneda, Y., Taira, A., 2012. Coseismic fault rupture at the trench axis
431 during the 2011 Tohoku-oki earthquake. *Nat. Geosci.* 5,

432 doi:10.1038/NGEO1547.

433 Koyi, H., 1995. Mode of internal deformation of sand wedges. *J. Struct. Geol.*17,
434 293-300.

435 Lallemand, S. E., Schnürle, P., Malavieille, J., 1994. Coulomb theory applied to
436 accretionary and nonaccretionary wedges: Possible causes for tectonic
437 erosion and/or frontal accretion. *J. Geophys. Res.* 99, 12033-12055.

438 Lallemand, S. E., Malavieille, J., Calassou, S., 1992. Effects of oceanic ridge
439 subduction on accretionary wedges: experimental modeling and marine
440 observations. *Tectonics*, 11(6), 1301-1313.

441 Malavieille, J., 1984. Modelisation experimentale des chevauchements
442 imbriques; application aux chaines de montagnes. *Bull. Soc. Géol. Fr.*, (1),
443 129-138.

444 Mandal, N., Chattopadhyay, A., Bose S., 1997. Imbricate thrust spacing:
445 experimental and theoretical analyses. In: Sengupta, S. (Ed.), *Evolution of*
446 *Geological Structures in Micro- to Macro-Scales*. Chapman and Hall,
447 London, 143 .

448 Mulugeta, G., 1988. Modeling the geometry of Coulomb thrust wedges. *J.*
449 *Struct.Geol.*10, 847.

450 Nakamura, Y., Kodaira, S., Miura, S., Regalla, C., Takahashi,N., 2013. High
451 resolution seismic imaging in the Japan Trench axis area of Miyagi,
452 Northeastern Japan. *Geophys. Res. Lett.* 40, 1713-1718.
453 doi:10.1002/grl.50364.

454 Pacheco,J.F.,Sykes,L.R.,Scholtz,C.H.,1993. Nature of seismic coupling along
455 simple plateboundaries of the subduction type.*J.Geophys.Res.*98,14133-
456 14159.

457 Park, J. O., Tsuru, T., Kaneda, Y., Kono, Y., Kodaira, S., Takahashi, N.,
458 Kinoshita, H., 1999. A subducting seamount beneath the Nankai
459 accretionary prism off Shikoku, southwestern Japan. *Geophys. Res.*
460 *Lett.*, 26(7), 931-934.

461 Persson, K.S., Sokoutis, D., 2002. Analogue models of orogenic wedges
462 controlled byerosion. *Tectonophysics.* 356, 323 .

463 Schellart, W. P., 2000. Shear test results for cohesion and friction coefficients for

464 different granular materials: scaling implications for their usage in
465 analogue modelling. *Tectonophysics*. 324.1, 1-16.

466 Souloumiac, P., Mailot B., Leroy, Y.M., 2012. Bias due to side wall friction in sand
467 box experiments, *J. Struct. Geol.*, 35, 90 - 101.

468 Storti, F., McClay, K.R., 1995. Influence of syntectonic sedimentation thrust
469 wedges in analogue models. *Geology*23, 999.

470 Strasser, M., Kölling, M., dos Santos Ferreira, C., Fink, H.G., Fujiwara, T.,
471 Henkel, S., Ikehara, K., Kanamatsu, T., Kawamura, K., Kodaira, S.,
472 Römer, M., Wefer, G., the R/V *Sonne* Cruise SO219A and JAMSTEC
473 Cruise MR12-E01 scientists., 2013. A slump in the trench: Tracking the
474 impact of the 2011 Tohoku- Okiearthquake. *Geology*.41,935-938.

475 Tanioka, Y., Ruff, L., Satake, K., 1997. What controls the lateral variation of large
476 earthquake occurrence along the Japan Trench? *IslandArc*. 6,261-266.

477 Tsuru, T., Park, J. O., Miura, S., Kodaira, S., Kido, Y., Hayashi, T., 2002. Along
478 - arc structural variation of the plate boundary at the Japan Trench margin:
479 Implication of interplate coupling. *J. Geophys. Res.* 107(B12), ESE-11, 1-
480 15.

481 von Huene, R., Culotta, R., 1989. Tectonic erosion at the front of the Japan
482 Trench convergent margin. *Tectonophysics*. 160, 75-90.

483 von Huene, R., Lallemand, S., 1990. Tectonic erosion along the Japan and Peru
484 convergent margins. *Geol. Soc. Am. Bull.* 102. 704-720.

485 von Huene, R., Ranero, C. R., Vannucchi, P., 2004. Generic model of subduction
486 erosion. *Geology*. 32, 913-916.

487 vonHuene,R.,Klaeschen,D.,Fruehn,J., 1999.RelationbetweentheSubductingPlate
488 andSeismicityAssociatedwiththeGreat1964AlaskaEarthquake.*PureAppl.*
489 *Geophys.*154,575.

490 Wang, K., Hu, Y. (2006). Accretionary prisms in subduction earthquake cycles:
491 The theory of dynamic Coulomb wedge, *J. Geophys. Res.* B06410,
492 doi:10.1029/2005JB004094.

493 Yamada, Y., Baba, K., Matsuoka, T., 2006. Analogue and numerical modeling of
494 accretionary prisms with a decollement in sediments. In: Buitter, S. J. H. &
495 Schreurs (eds) *Analogue and numerical modeling of crustal- scale*

496 processes. Geol. Soc. London Spec. Pub, 253, 169-183.

497

498 **Figure Captions:**

499

500 **Figure 1:** (a) Location map, showing the eastern coastline of Honshu, bathymetry

501 near Japan Trench and Tohoku earthquake epicenter (red star). The yellow arrow

502 indicates the direction of plate convergence. Inset map shows location of Expedition

503 343 site C0019 (red star) along seismic section Line HD 33B (Fig.1b). Line HD 26B

504 another seismic section line shown in figure 1c. (b) Image of seismic section Line HD

505 33B crossing the IODP drilling site C0019 with no vertical exaggeration. It shows

506 change in topographic slope (marked red lines) from inner wedge ($\sim 10^\circ$) to outer

507 wedge ($\sim 4^\circ$) (modified after Nakamura et al., 2013). (c) Image of seismic section

508 Line 26B with V.E. ~ 3 , separated by 3.5 km from seismic line HD 33B. α_i and α_o are

509 relative slopes of inner and outer wedges respectively, showing changes in

510 topographic slope (modified after Nakamura et al., 2013). Pink line marks the

511 decollement surface and blue arrow indicates the zone of topographic slope-break in

512 both (b) and (c).

513 **Figure 2:** A sketch of the experimental setup showing 3D view of the model setup.

514 Zones I and II represent low and high frictional contact zone respectively. Arrows on

515 the right show the direction of shortening.

516 **Figure 3:** Progressive development of frontal wedge in sand models with 10 cm

517 width of the Zone II. (a) Initial model, (b-e) Initial stage, (f) intermediate stage and

518 (g-h) progressive development of wedge during the final stage (see text for details).

519 Note that the deformation propagation towards front stopped after shortening of 14.

520 40 cm, but hinterland elevation continued to increase (e). 18.10 cm shortening was

521 accommodated within the wedge, reorienting earlier structures during intermediate

522 stage (f). Further shortening moves the deformation front above the lower frictional
523 base developing distinct slope-break (g-h).

524 **Figure 4:** Plots show different stages of wedge growth for varying width of zone II
525 using high frictional patch (7 experiments) and rigid block (4 experiments). Wedge
526 angle (a) and Wedge height at the backstop (b), are plotted as a function of actual
527 displacement (horizontal shortening) in cm. In the initial stage of the wedge growth,
528 wedge angle (a) and wedge height (b) reached a constant value with horizontal
529 displacement. The intermediate stage marks the sharp increase in both wedge angle
530 (solid line) (a) and wedge height (solid line) (b). In the final stage wedge height
531 attained a constant value (dash line) (b) with decreasing wedge slope (dash line) (a).

532 **Figure 5:** Final stage of wedge development for varying widths of high frictional
533 patch: 2 cm (a), 4 cm (b), 6 cm (c), 10 cm (d), 12 cm (e), 14 cm (f) and 30 cm (g). The
534 width of the model is 35 cm for all experiments. White arrow marks the zone of
535 topographic slope-break between inner and outer wedge.

536 **Figure 6:** Progressive development of frontal wedge growth over multiple high
537 frictional patch, forming alternate uniform slope and topographic slope-break. (a-d)
538 Initial stage, (e) intermediate stage with steep uniform slope, (f-g) final stage showing
539 the development of slope-break, (h) the process of destruction of outer wedge
540 observed in figure (g) due to another high frictional in the front, leading to steep
541 uniform surface slope (i), (j) development of new slope-break in the wedge geometry
542 low basal friction, (k) Plots show the variations of wedge angle (purple) and wedge
543 elevation at the hinterland buttress (green) as a function of horizontal displacement.
544 Note that the combination of low tapered wedge at constant wedge elevation implies
545 growing of wedge over low frictional base (yellow shade).

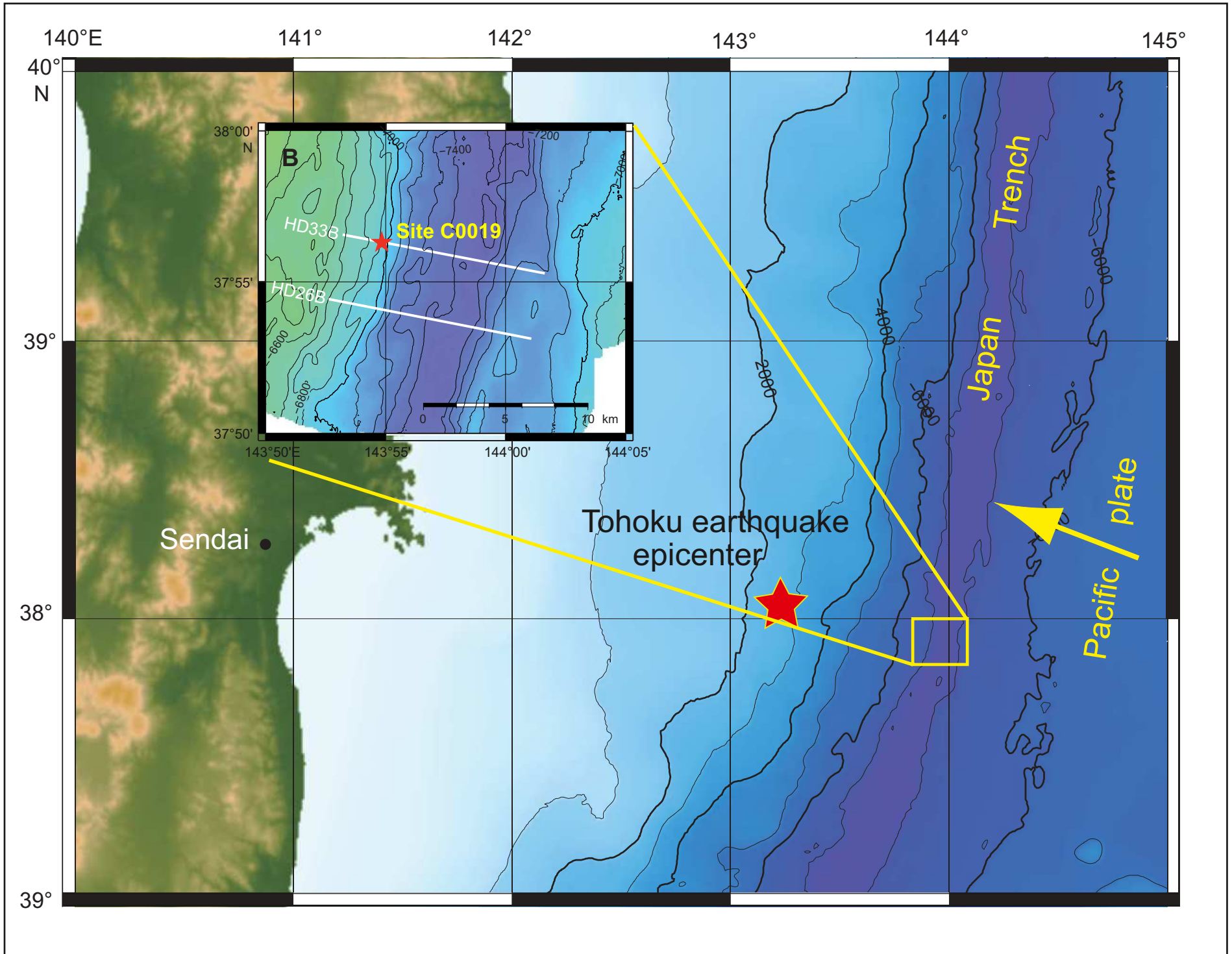
546 **Figure 7:** Compilation of core data with depth at IODP sites C0019 and comparison

547 with experimental model. (a) Deformation unit in the core data shows variations in
548 bedding dip with depth and three structural domains are identified. (i) upper frontal
549 prism (0-275 mbsf) shows gently inclined bedding, (ii) lower frontal prism (276-820
550 mbsf) showing variable and steeply dipping beds characterized by folded and faulted
551 sediments, (iii) base section (820 mbsf to base of the hole) with shallow to horizontal
552 bedding represents in the footwall block in the subduction zone (modified after
553 Chester et al., 2013). (b) Experimental model shows resemblance in the changes of
554 bedding orientations with depth. Green arrows show the region in the experimental
555 model comparable with core data set. White dash line in the model replicates the
556 drilling site C0019 shown in Fig. 7c. (c) Details and interpretations of seismic image
557 along section HD 33B. Vertical Exaggeration = 2:1 (Modified after Kodaira et al.,
558 2012). Note that experimental model closely reproduces geometrical and structural
559 features observed in seismic image. Both experimental and seismic section show that
560 surface slope of the inner wedge is steeper than that of the outer wedge. Imbricate
561 thrusts are prominent within the outer wedge. The blue arrow marks the zone of
562 topographic slope-break between inner and outer wedges in Figs. 7b and 7c.

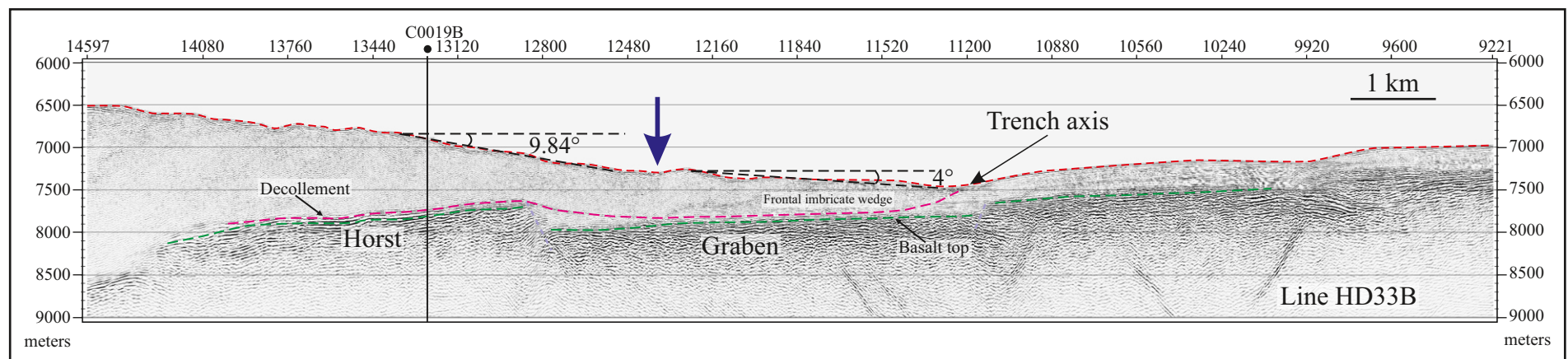
Table 1
Modeling Parameters and material properties

Parameter and model properties	Sand (analogue model)	Natural prototypes	Ratio: model/nature
Length, L (m)	0.01	360	$\lambda = 2.7 \times 10^{-5}$
Density (kg m ⁻³)	1600	2700	$\delta = 0.59$
Internal friction angle, ϕ (°)	~ 30	30 - 40	1 - 0.75
Cohesion (Pa)	20	2×10^6	1×10^{-5}
Gravity, g (m s ⁻²)	9.8	9.8	$\gamma_g = 1$
Deviatoric Stress * ($\sigma = \delta \cdot g \cdot L$)	157 Pa	$9.5 \cdot 10^6$	16.5×10^{-6}

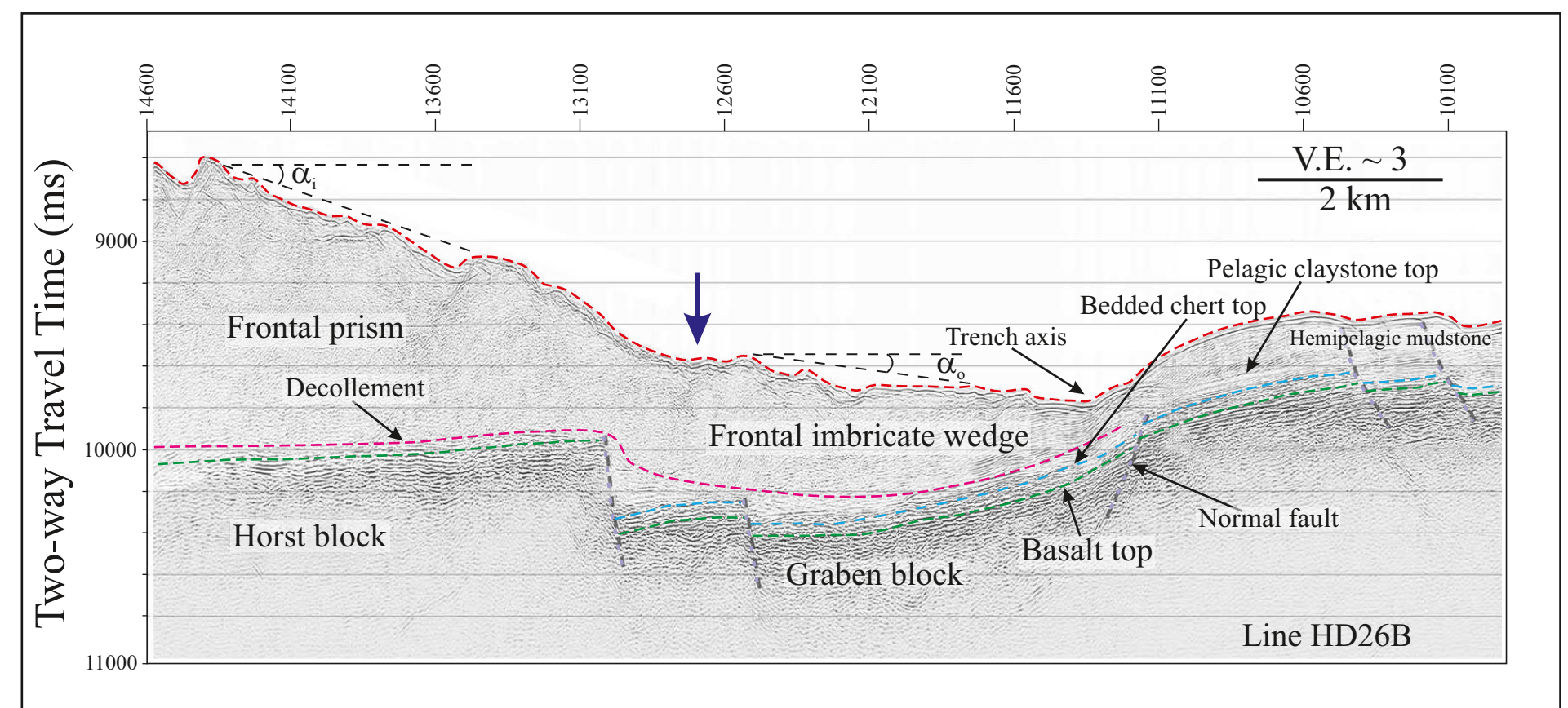
* Based on Schellart, 2000



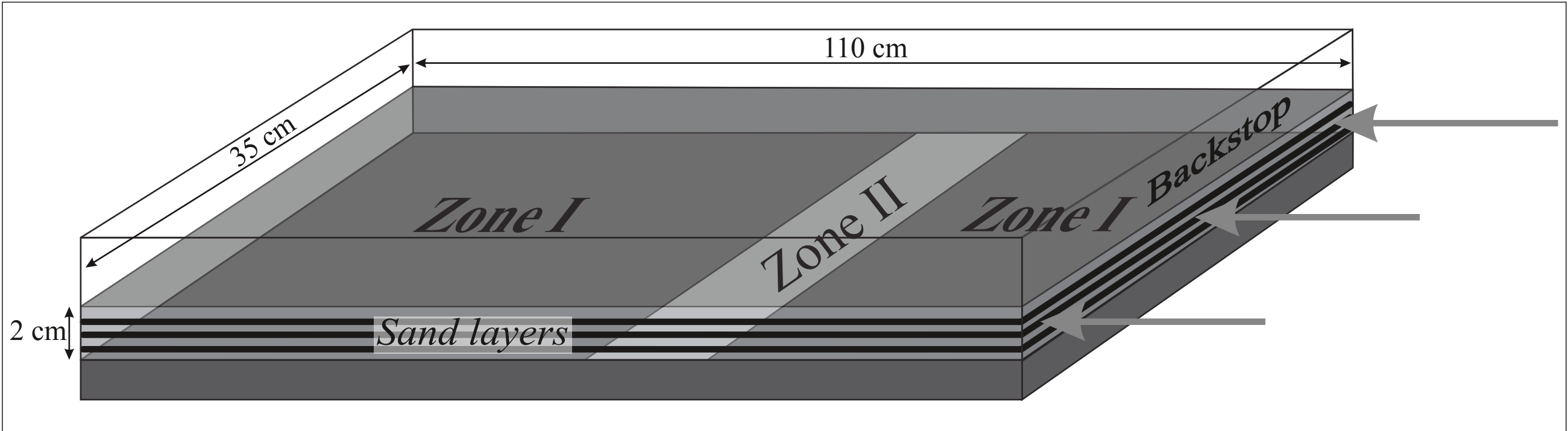
a

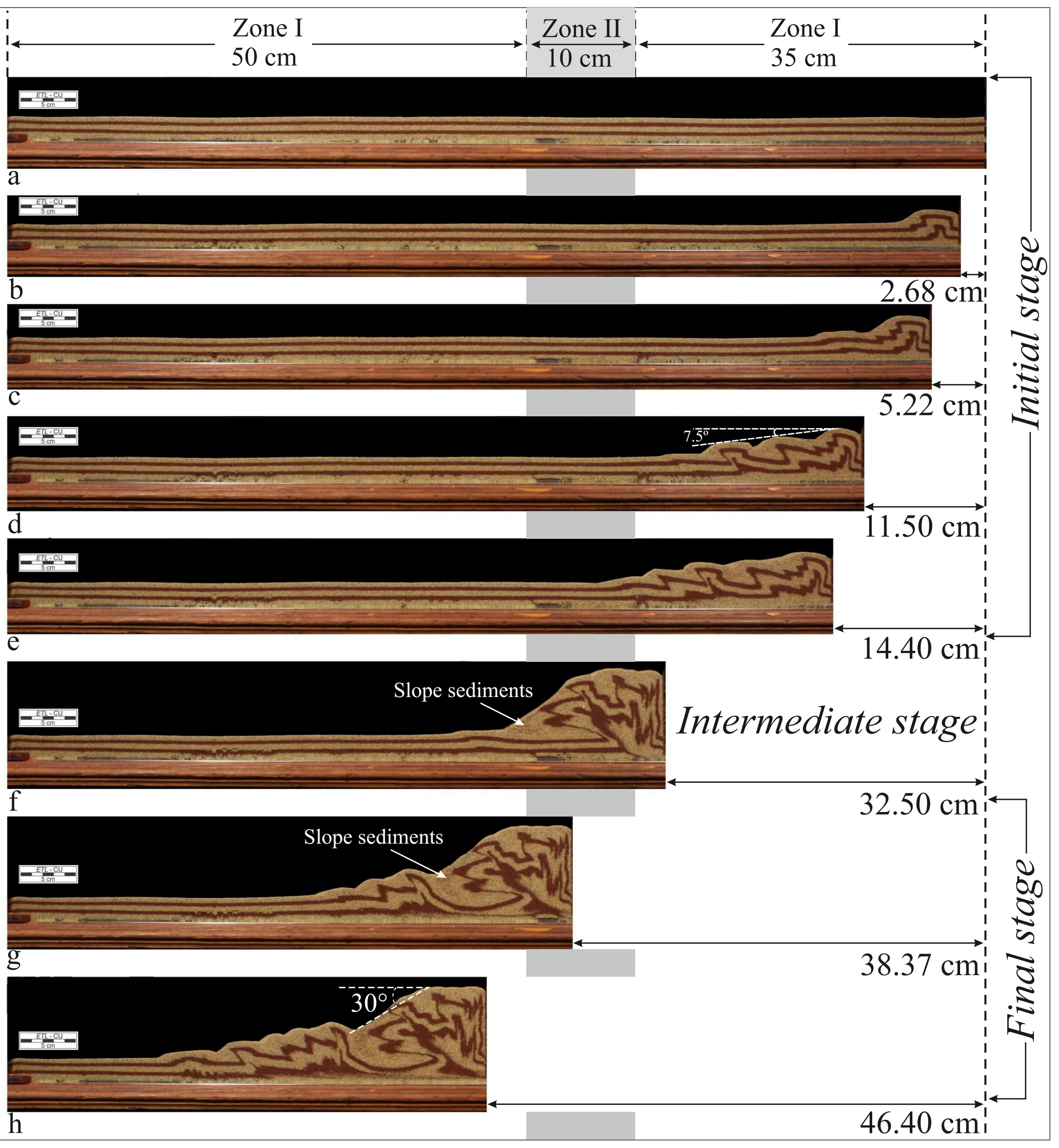


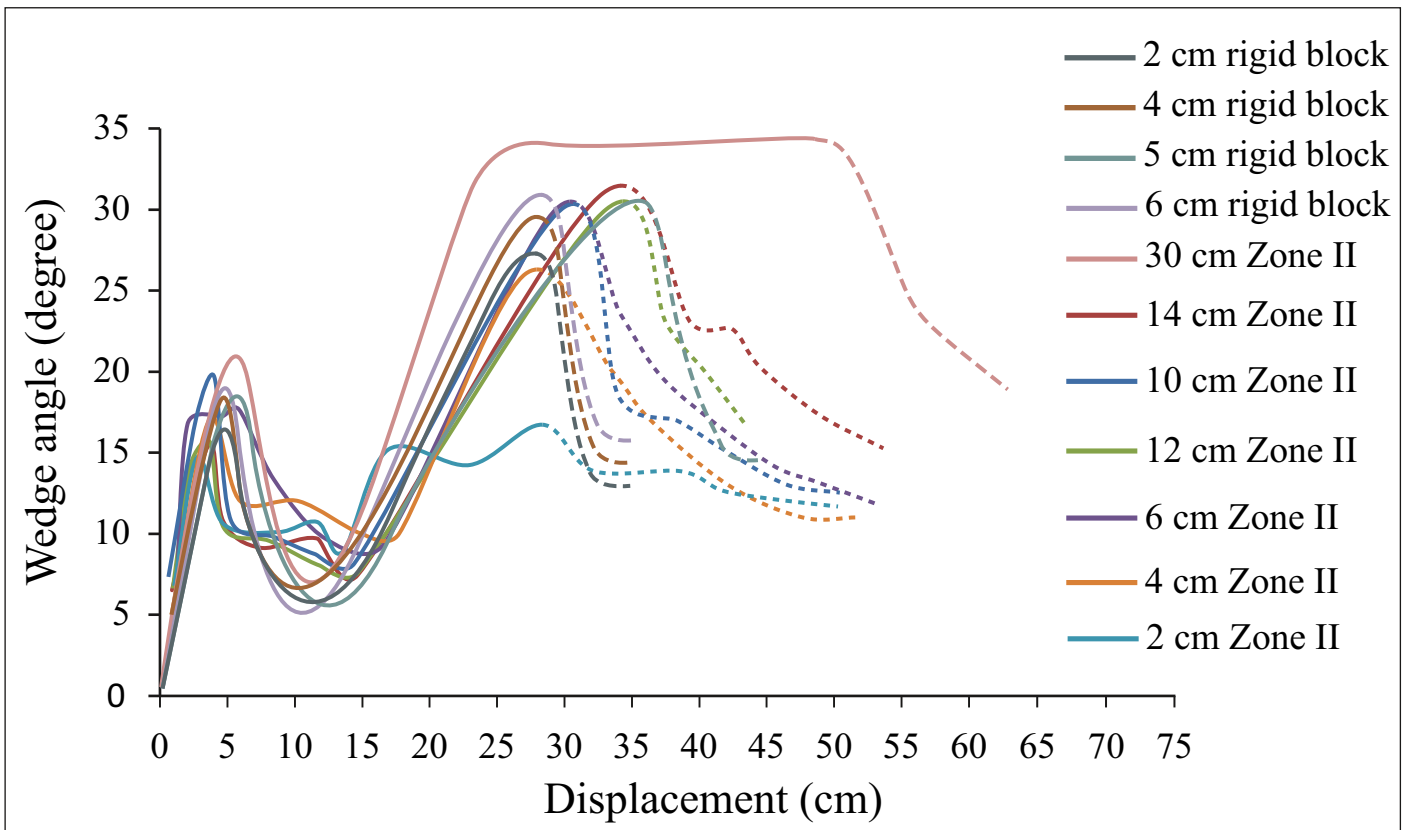
b



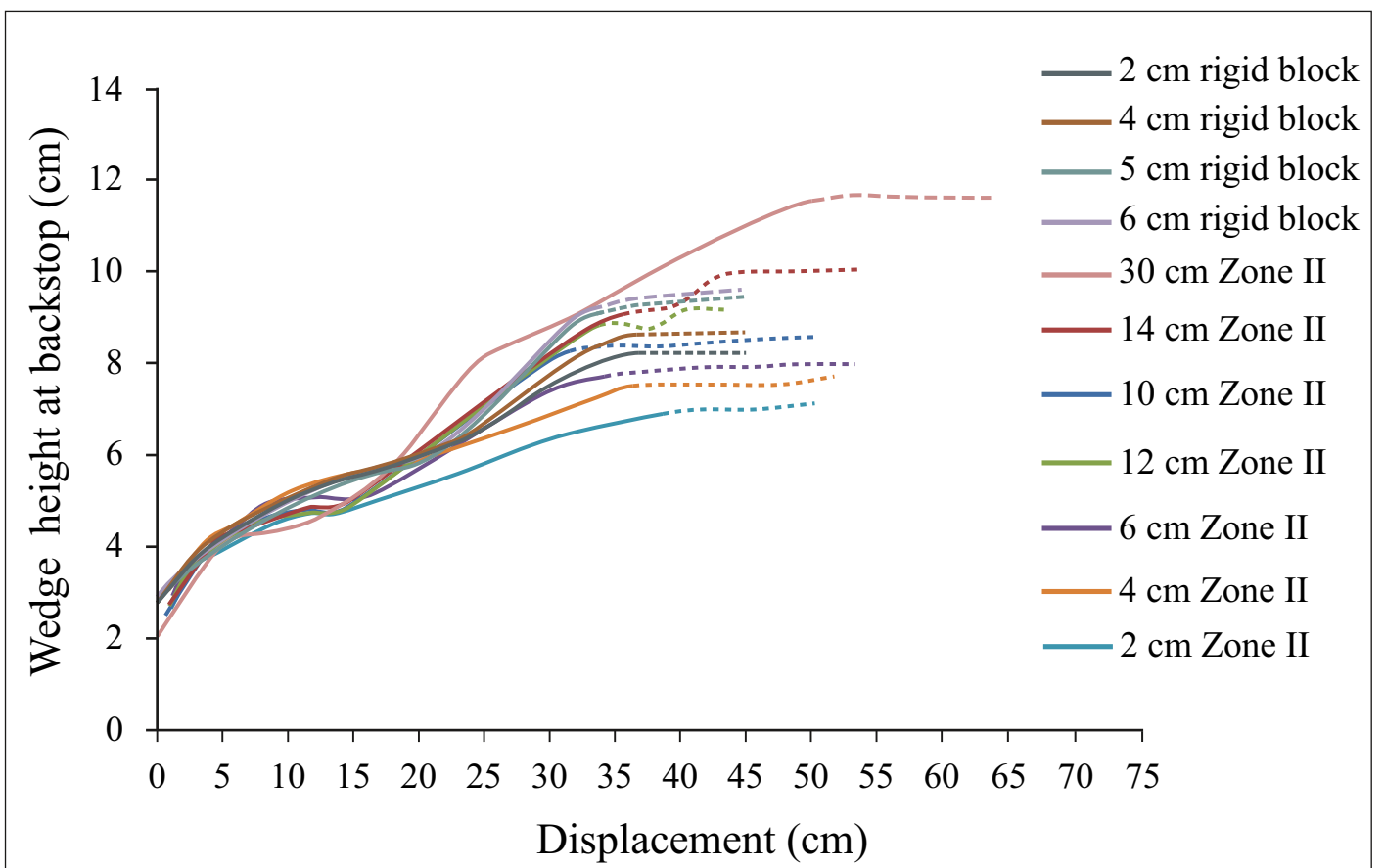
c



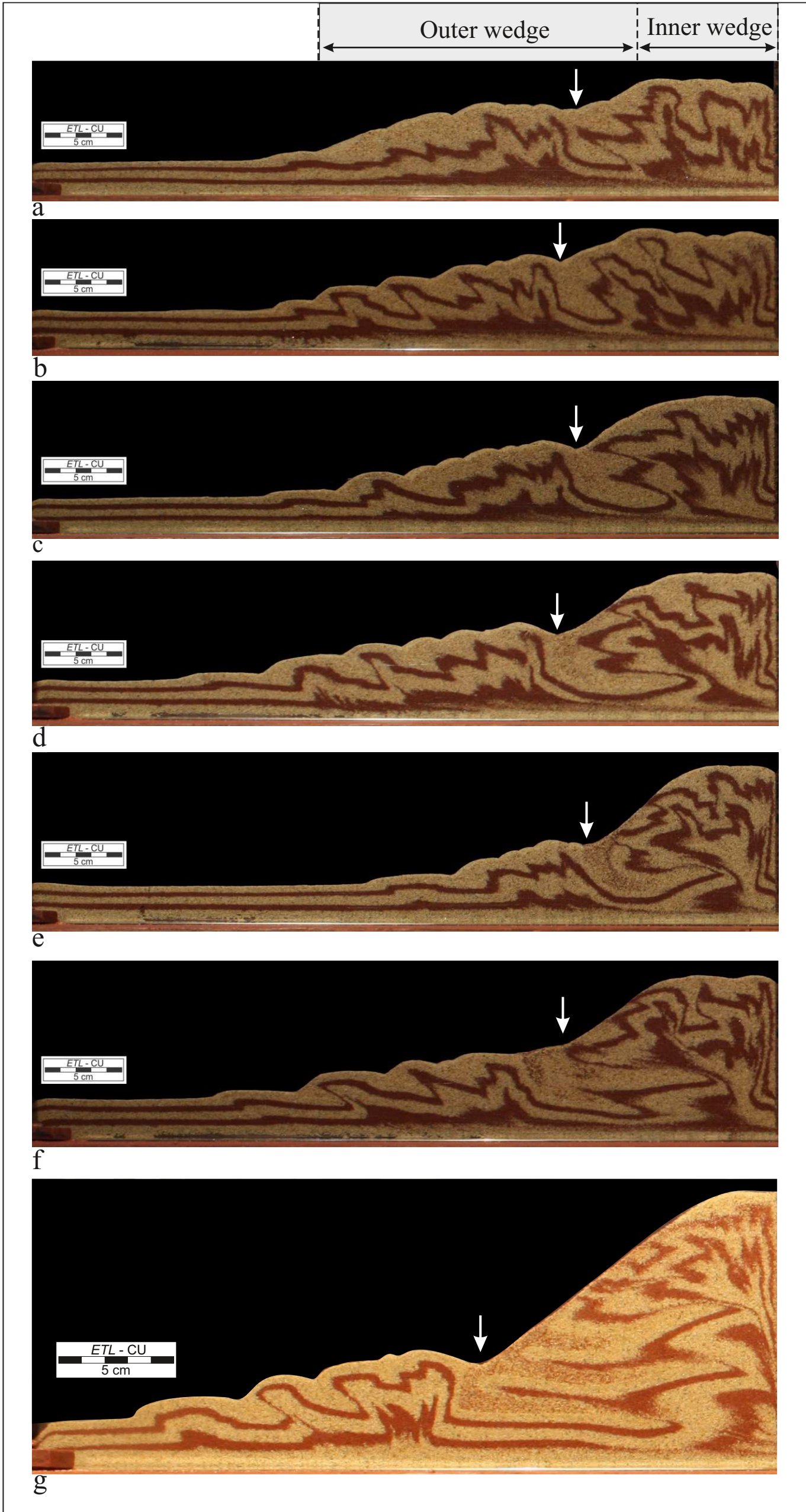


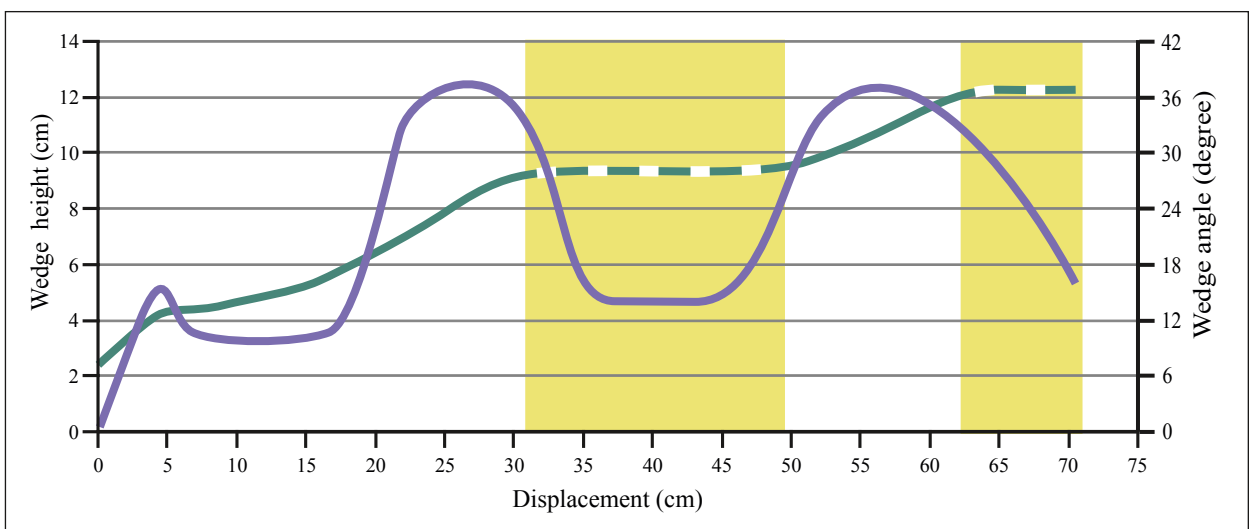
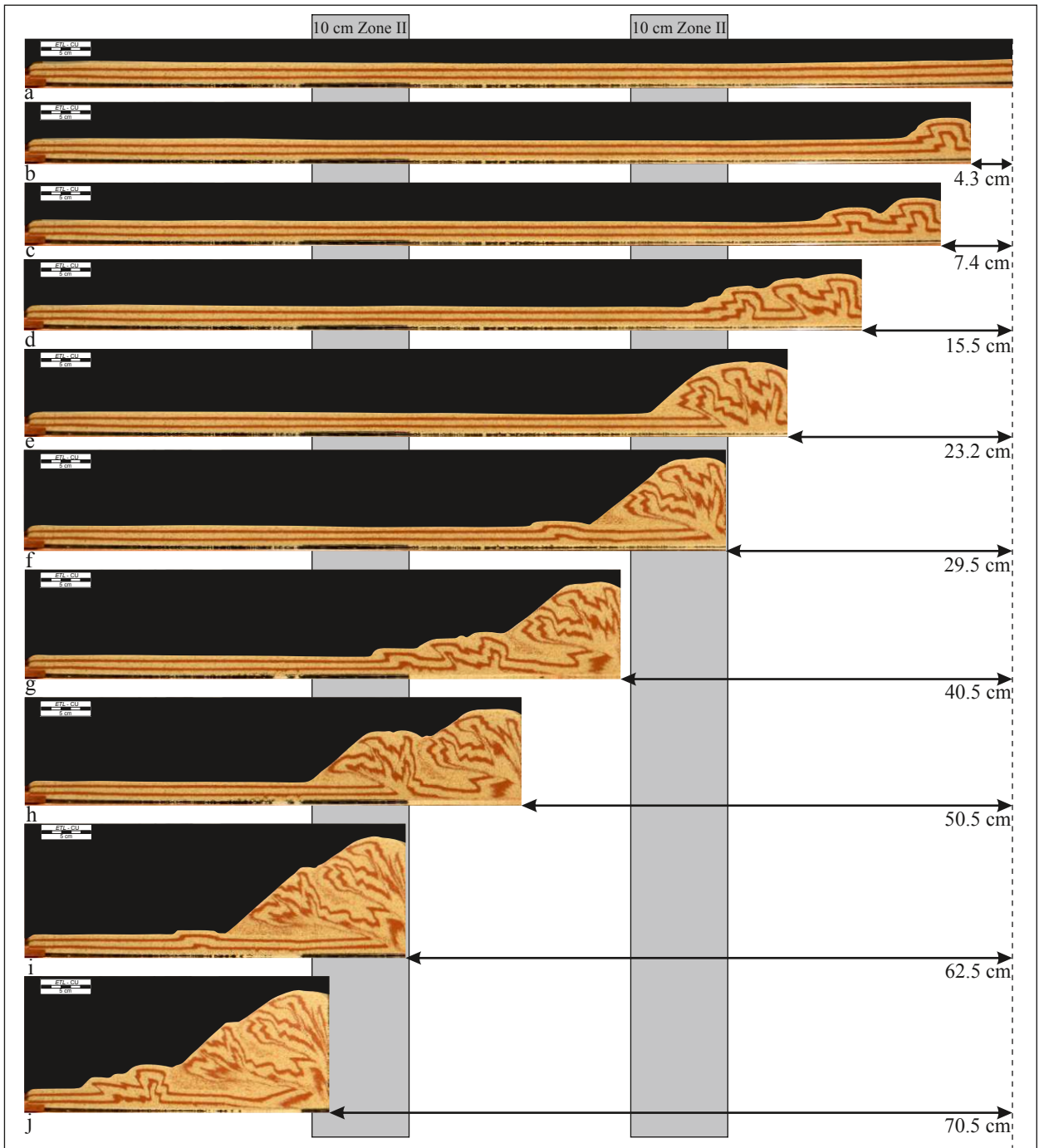


a



b





k

